Solvothermal Synthesis, Structure, and Properties of Metal Organic Framework Isomers Derived from a Partially Fluorinated Link

ARTICLE *in* CRYSTAL GROWTH & DESIGN · FEBRUARY 2011

Impact Factor: 4.89 · DOI: 10.1021/cg101414x

4 AUTHORS:

Pradip S Pachfule
CSIR - National Chemical Laboratory, Pune
44 PUBLICATIONS **1,028** CITATIONS
SEE PROFILE

Raja Das
CSIR - National Chemical Laboratory, Pune
35 PUBLICATIONS **663** CITATIONS
SEE PROFILE

Pankaj Poddar
CSIR - National Chemical Laboratory, Pune
129 PUBLICATIONS **2,419** CITATIONS
SEE PROFILE

Rahul Banerjee
CSIR - National Chemical Laboratory, Pune
126 PUBLICATIONS **5,888** CITATIONS
SEE PROFILE

CRYSTAL GROWTH & DESIGN

ARTICLE

pubs.acs.org/crystal

Solvothermal Synthesis, Structure, and Properties of Metal Organic Framework Isomers Derived from a Partially Fluorinated Link

Published as part of a virtual special issue on Structural Chemistry in India: Emerging Themes

Pradip Pachfule, Raja Das, Pankaj Poddar, and Rahul Banerjee*

Physical/Materials Chemistry Division, National Chemical Laboratory, Dr. Homi Bhabha Road, Pune-411008, India

Supporting Information

ABSTRACT: Solvothermal reactions of $Cu(NO_3)_2 \cdot 3H_2O$ with 4,4′-(hexafluoroisopropylidene) bis(benzoic acid) ($C_{17}H_{10}F_6O_4$, H_2hfbba) and terminal monodentate ligand 3-methyl pyridine (3-picoline/3-mepy) in the presence of *N*, *N*-dimethyl formamide (DMF) and *N*,*N*-diethyl formamide (DEF) solvents gave rise to two structurally different two-dimensional (2D) fluorinated metal organic frameworks (*F*-MOFs). The effect of the choice of solvent has been clearly reflected in the structures obtained. The *F*-MOFs reported in this paper are formulated as $[Cu_2(hfbba)_2(3\text{-mepy})_2] \cdot (DMF)_2(3\text{-mepy})$ (***F*-MOF-4**), $[Cu_2(hfbba)_2(3\text{-mepy})_2]$ (**Cu-*F*-MOF-4B**), and $[Zn_2(hfbba)_2(3\text{-mepy})_2] \cdot (3\text{-mepy})$ (**Zn-*F*-MOF-4B**) which displays interesting 2D structures with and without interdigitation depending on the solvent used. The structures of these *F*-MOFs have been determined by X-ray crystallography and further identified by IR spectroscopy, powder X-ray diffraction (PXRD), and thermogravimetric analysis (TGA). The effect of interdigitation has been reflected in the gas adsorption and magnetic properties of these *F*-MOFs. These *F*-MOFs also show comparable H_2 and CO_2 uptake depending on their structural variation. Temperature-dependent magnetic susceptibility measurements over a wide range of temperatures exhibit dominantly short-range antiferromagnetic behavior, with weak ferromagnetic behavior showing up at very low temperatures, which is evident from opening of the hysteresis loop with a finite value of coercivity in both *F*-MOF-4 and Cu-*F*-MOF-4B. We observed a smaller value of μ_{eff} per Cu atom and coercivity in Cu-*F*-MOF-4B than the *F*-MOF-4 due to relatively larger distances between the neighboring dicopper paddlewheel secondary building unit.

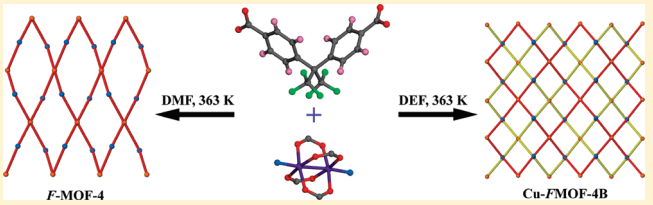

INTRODUCTION

Metal−organic frameworks (MOFs) have emerged as a new class of crystalline porous materials with adsorption capacities and pore sizes (for porous MOFs) exceeding traditional porous materials such as zeolites and porous carbon.[1] MOFs are considered promising material with potential for major impact in hydrogen storage,[2] carbon sequastration,[3] heterogeneous catalysis,[4] multiferroics,[5] and drug delivery.[6] Among these applications, the origin of magnetic and ferroelectric ordering (as well as the coexistence of both) has significant potential in the future. In MOFs, the magnetic ordering, which is a cooperative phenomenon, arises from the effective magnetic interaction between the paramagnetic centers through the organic bridging groups of the framework. The construction of different types of frameworks with variable intermetal center distances and their bond angles can give rise to antiferro/ferromagnetic ordering or spin-glass behavior. Moreover, it enriches understanding of the mechanism behind long-range ordering, spin frustration, metamagnetism, anisotropy, etc. Cu-based MOFs are particularly interesting due to their versatile magnetic interaction with different arrangements of metal centers via a variety of ligands.[5f,g] Hydrogen and carbon dioxide storage capacity in MOFs can be enhanced in various ways, such as introducing open metal sites, cation exchange, functionalizing organic linkers, and utilizing catenation.[7] Recently, researchers have explored the possibility of synthesizing fluorinated metal organic frameworks (*F*-MOFs), using perfluorinated polycarboxylate, ligands with porous surfaces, and exposed fluorine atoms for interesting H_2 and CO_2 storage properties.[8,9] However, there are only a few reports of *F*-MOFs in the literature as perfluorinated carboxylic acids are significantly more acidic than nonfluorinated carboxylic acids, and subsequently less soluble in common organic solvents. Fluorinated acids are also less stable than their nonfluorinated analogues, and it has been found that they often decompose at temperatures commonly used to form MOFs of higher dimensionality (125−180 °C).

As a part of our ongoing investigation on the synthesis of different *F*-MOFs,[9] we studied the hydrothermal chemistry of a perfluorinated bent ligand 4,4′-(hexefluoroisopropylidine) bis-(benzoic acid) (H_2hfbba), with the N donor monodentate coligand 3-methyl pyridine (3-picoline) using transition metal centers as Cu^{2+} and Zn^{2+} in the presence of *N*,*N*-dimethyl

Received: October 22, 2010
Revised: January 28, 2011
Published: February 22, 2011

dx.doi.org/10.1021/cg101414x | *Cryst. Growth Des.* 2011, 11, 1215–1222

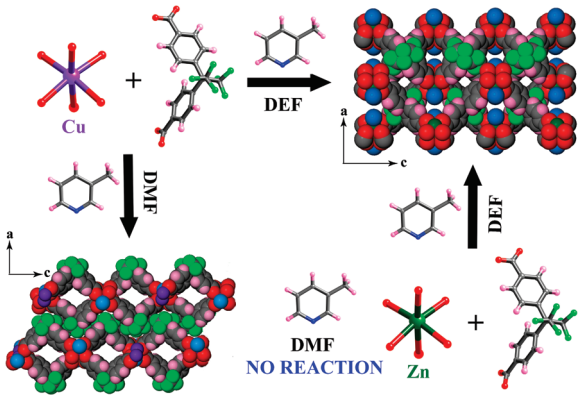

Figure 1. Synthetic details and scheme of synthesis of all the *F*-MOFs reported in this paper.

formamide (DMF) and *N*,*N*-diethyl formamide (DEF) solvents. Although MOF synthesis, in general, occurs in solvothermal media (water, organic solvents, ionic liquids),[10] none of the synthetic details described in the literature explain the cause behind the solvent choice, despite it being an important parameter in the synthesis of a desired phase. The *F*-MOFs[11] reported in this paper are formulated as $[Cu_2(hfbba)_2(3\text{-mepy})_2]\cdot(DMF)_2(3\text{-mepy})$ (***F*-MOF-4**), $[Cu_2(hfbba)_2(3\text{-mepy})_2]$ (**Cu-*F*-MOF-4B**) and $[Zn_2(hfbba)_2(3\text{-mepy})_2]\cdot(3\text{-mepy})$ (**Zn-*F*-MOF-4B**) which displays interesting two-dimensional (2D) structures with and without interdigitation depending on the solvent used (Figure 1).[12] The structure of these *F*-MOFs have been determined by X-ray crystallography and further identified by IR spectroscopy, powder X-ray diffraction (PXRD), and thermogravimetric analysis (TGA). ***F*-MOF-4** and **Cu-*F*-MOF-4B** show interesting magnetic properties although both contain the same dicopper paddlewheel secondary building unit (SBU) as joints and hfbba ligand as links between the joints. These *F*-MOFs also show comparable H_2 and CO_2 uptake depending on their structural variation.

EXPERIMENTAL SECTION

General Procedures. All reagents and solvents for synthesis and analysis were commercially available and used as received. The Fourier transform (FT) IR spectra (KBr pellet) were taken on a PERKIN ELMER FT-IR SPECTRUM (Nicolet) spectrometer. PXRD patterns were recorded on a Phillips PANalytical diffractometer for Cu Kα radiation (λ = 1.5406 Å), with a scan speed of 2° min^{-1} and a step size of 0.02° in 2θ. TGA experiments were carried out in the temperature range of 15−800 °C on a SDT Q600 TG-DTA analyzer under N_2 atmosphere at a heating rate of 10 °C min^{-1}. All low pressure gas adsorption experiments (up to 1 bar) were performed on a Quantachrome Quadrasorb automatic volumetric instrument.

Synthesis of $[Cu_2(hfbba)_2(3\text{-mepy})_2]$ (Cu-F-MOF-4B). 0.5 mL of 3-methyl pyridine stock solution and 1.5 mL of H_2hfbba solution (0.20 M) in DEF were mixed in a 5 mL vial. 0.5 mL of $Cu(NO_3)_2\cdot3H_2O$ solution (0.20 M) in DEF was added to this solution. The vial was capped and heated to 85 °C for 96 h. The mother liquor was decanted and the products were washed with DEF (15 mL) three times. Dark blue colored crystals of **Cu-*F*-MOF-4B** were collected by filtration and dried in air (10 min). [Yield: 67%, 0.0161 g depending on $Cu(NO_3)_2\cdot3H_2O$]. FT-IR: (KBr 4000−450 cm^{-1}): 3659(m, br), 3071(m, br), 2935(w), 1632(m), 1407(s), 1239(m), 1173(s), 929(m), 779(m), 514(m).

$[Cu_2(hfbba)_2(3\text{-mepy})_2]\cdot(DMF)_2(3\text{-mepy})$ (F-MOF-4)[9b]. 0.5 mL of 3-methyl-pyridine stock solution (0.20 M) and 1.5 mL of H_2hfbba stock solution in DMF (0.20 M) were mixed in a 5 mL vial. 0.5 mL of $Cu(NO_3)_2\cdot3H_2O$ stock solution (0.20 M) was added to this solution. The vial was capped and heated to 85 °C for 96 h. The mother liquor was decanted and the products were washed with DMF (15 mL) three times. Blue colored crystals of ***F*-MOF-4** were collected by filtration and dried in air (10 min). [Yield: 50%, 0.0121 g depending on $Cu(NO_3)_2\cdot3H_2O$]. FT-IR: (KBr 4000−400 cm^{-1}): 3676(br), 3068(w), 3935(m), 2657(w), 2548(w), 2331(s), 1944(m), 1816(w), 1683(m), 1632(w), 1561(w), 1410(s), 1291(w), 1239(s), 1174(w), 1090(w), 1020(w), 971(w), 929(w), 846(m), 780(s), 748(w), 706(w), 514(m), 494(w).

Synthesis of $[Zn_2(hfbba)_2(3\text{-mepy})_2]\cdot(3\text{-mepy})$ (Zn-FMOF-4B). 0.5 mL of 3-methyl pyridine stock solution and 1.5 mL of H_2hfbba solution (0.20 M) in DEF were mixed in a 5 mL vial. 0.5 mL of $Zn(NO_3)_2\cdot6H_2O$ solution (0.20 M) in DEF was added to this solution. The vial was capped and heated to 85 °C for 96 h. The mother liquor was decanted and the products were washed with DEF (15 mL) three times. Colorless crystals of **Zn-*F*-MOF-4B** were collected by filtration and dried in air (10 min). [Yield: 48%, 0.0142 g depending on $Zn(NO_3)\cdot6H_2O$]. FT-IR: (KBr 4000−450 cm^{-1}): 3310(m, br), 2941(w), 1938(w), 1644(s), 1570(m), 1410(s), 1291(m), 1174(m), 929(m), 780 (m), 477(m).

X-ray Crystallography. All single crystal data were collected on a Bruker SMART APEX three circle diffractometer equipped with a CCD area detector (Bruker Systems Inc., 1999a)[13] and operated at 1500 W power (50 kV, 30 mA) to generate Mo Kα radiation (λ = 0.71073 Å). The incident X-ray beam was focused and monochromated using Bruker Excalibur Gobel mirror optics. Crystals of the *F*-MOFs reported in the paper were mounted on nylon CryoLoops (Hampton Research) with Paraton-N (Hampton Research). Data were integrated using Bruker *SAINT* software.[14] Data were subsequently corrected for absorption by the program *SADABS*.[15] The space group determinations and tests for merohedral twinning were carried out using *XPREP*.[16] In all cases, the highest possible space group was chosen. All structures were solved by direct methods and refined using the *SHELXTL 97* software suite.[17] Atoms were located from iterative examination of difference F-maps following least-squares refinements of the earlier models. Hydrogen atoms were placed in calculated positions and included as riding atoms with isotropic displacement parameters 1.2−1.5 times U_{eq} of the attached C atoms. Data were collected at 298(2) K for all the *F*-MOFs reported in this paper. All structures were examined using the *ADDSYM* subroutine of *PLATON*[18] to ensure that no additional symmetry could be applied to the models. **Zn-*F*MOF-4B** has been solved and refined in a space group $Cmc2_1$ (see section S2 in Supporting Information for the coordinates) although a solution could be obtained for space group *Cmca* (see section S2 in Supporting Information for the coordinates). However, all our efforts to refine the structure in Cmca space group were unsuccessful. As a result, the space group $Cmc2_1$ has been chosen. High degree of mosaicity, possible pseudosymmetry, or a possible twining could be the cause of this effect. We acknowledge the fact that no suitable crystal for **Zn-*F*MOF-4B** with good diffraction could be obtained. The crystal structure of **Cu-*F*MOF-4B**, which has a similar unit cell dimension as **Zn-*F*MOF-4B**, could be solved and refined in *Cmca* space group. All ellipsoids in ORTEP diagrams are displayed at the 50% probability level unless noted otherwise. Supporting Information contains a detailed data collection strategy and crystallographic data for the two *F*-MOFs reported in this paper. Crystal data and details of data collection, structure solution, and refinement are summarized in Table 1. Crystallographic data (excluding structure factors) for the structures reported in this paper have been deposited with the CCDC as deposition no. CCDC 797251, 797252 (see also Table 1). Copies of the data can be obtained, free of charge, on application to the CCDC, 12 Union Road, Cambridge CB2 lEZ UK (fax: + 44 (1223) 336 033; e-mail: deposit@ccdc.cam.ac.uk).

H_2 and CO_2 Adsorption Measurements. Hydrogen adsorption−desorption experiments were conducted at 77 K using a

Table 1. Crystal Data and Structure Refinement for *F*-MOFs Reported in This Paper

	Cu-*F*MOF-4B	*F*-MOF-4	Zn-*F*MOF-4B
empirical formula	C23 H15 O4 F6 N Cu	C29.97 H27.97 F6 N2.91 O5.5 Cu	C29 H22 F5.92 N2 O4 Zn
formula weight	546.91	694.51	640.36
temperature (K)	293(2)	100(2)	293(2)
wavelength (Å)	0.71073	0.71073	0.71073
crystal system	orthorhombic	monoclinic	orthorhombic
space group	*Cmca*	*P*2(1)/c	*Cmc21*
unit cell dimensions	a = 21.561(3) Å	a = 25.643(8) Å	a = 21.626(2) Å
	b = 14.717(2) Å	b = 11.004(3) Å	b = 14.662(17) Å
	c = 17.745(3) Å	c = 24.351(7) Å	c = 17.777(3) Å
		β = 115.518°	
volume	5630.7(15)	6201.0(3)	5636.8(13)
Z	8	4	8
density (calculated)	1.290	1.488	1.507
goodness-of-fit on F^2	1.067	0.986	0.949
final R indices [$I > 2\sigma(I)$]	R_1 = 0.0529, wR_2 = 0.1410	R_1 = 0.0557, wR_2 = 0.1278	R_1 = 0.0596, wR_2 = 0.1345
R indices (all data)	R_1 = 0.0660, wR_2 = 0.1638	R_1 = 0.0990, wR_2 = 0.1439	R_1 = 0.0967, wR_2 = 0.1542

Quantachrome Quadrasorb automatic volumetric instrument. Ultrapure H_2 (99.9995%) was purified further by using calcium aluminosilicate adsorbents to remove trace amounts of water and other impurities before introduction into the system. For measurements at 77 K, a standard low-temperature liquid nitrogen Dewar vessel was used. CO_2 adsorption−desorption measurements were done at room temperature (293 K). Before gas adsorption measurements, the sample was activated at room temperature (for 24 h) and 100 °C (for 36 h) under ultrahigh vacuum (10^{-8} mbar) overnight. About 85 mg of samples were loaded for gas adsorption, and the weight of each sample was recorded before and after outgassing to confirm complete removal of all guest molecules.

Measurements of Magnetism. DC magnetization vs temperature measurements were performed for ***F*-MOF-4** and **Cu-*F*-MOF-4B** at 500 Oe in both field cooled (FC) and zero field cooled (ZFC) modes. For the FC & ZFC measurements, the sample was cooled down to 3 K in 500 Oe field and without field respectively, and data were collected while heating up in both cases at 2 K per minute at every second after averaging over 40 Hz. All the measurements were done using a Physical Property Measurement System (PPMS) from Quantum Design Inc. San Diego, USA, equipped with a 7 T superconducting magnet and a vibrating sample magnetometer. The magnetic signal from the sample holder was negligible to affect our data accuracy.

RESULTS AND DISCUSSION

Synthesis. The *F*-MOFs reported were synthesized solvothermally with 4,4′-(hexafluoroisopropylidene) bis(benzoic acid) (H_2hfbba) along with $M(NO_3)_2$ (M = Cu or Zn) as a metal center and 3-mepy as coligand in DEF and DMF as solvents (Figure 1). We synthesized these *F*-MOFs by using H_2hfbba because (a) its bent geometry and considerably long molecular backbones of such building block can induce formation of a porous framework with many characteristics such as selective gas adsorption, gas storage, catalysis and (b) the twisted conformation of this ligand may provide the ability to shape helical assembly with chirality in the resultant supramolecular architecture. In the resultant *F*-MOFs formed, ***F*-MOF-4** from DMF has a totally different crystal morphology from **Cu-*F*-MOF-4B** formed from DEF possibly due to the change in solvent. PXRD confirmed that we could also synthesize **Cu-*F*-MOF-4B** using H_2O (in place of DEF) as a solvent for synthesis. Reaction of H_2hfbba with 3-methyl pyridine and $Zn(NO_3)_2$ in the presence of DMF results in no reaction. However, a similar reaction in DEF as solvent produces **Zn-*F*-MOF-4B** as microcrystalline precipitate (Figure 1). We will first discuss the crystal structure of **Cu-*F*-MOF-4B** that has been synthesized in DEF and follow that by a discussion of ***F*-MOF-4** synthesized in DMF.

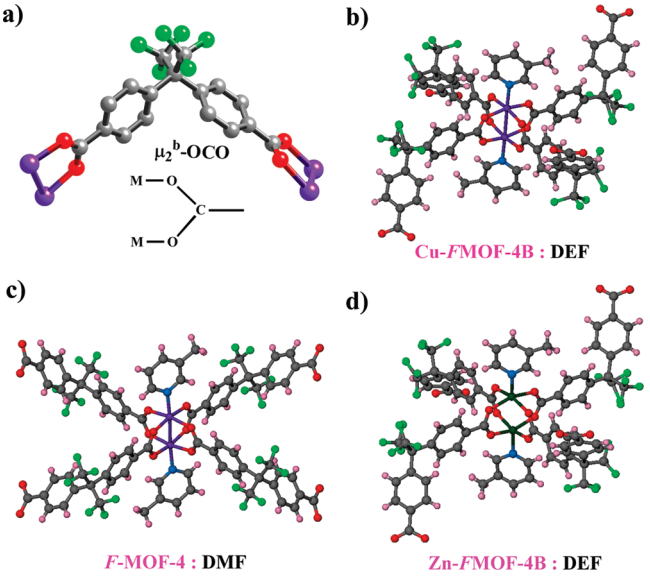

Figure 2. (a) $\mu_2{}^b$-OCO bridging mode observed in *F*-MOFs. (b) SBU of **Cu-*F*-MOF-4B**. (c) SBU of ***F*-MOF-4**. (d) SBU of **Zn-*F*-MOF-4B**. Color code: M (green/violet), N (blue), O (red), C (gray), F (light green).

Description of Crystal Structures. *Crystal Structure of [Cu_2(hfbba)$_2$(3-mepy)$_2$] (Cu-FMOF-4B).* The asymmetric unit of **Cu-*F*-MOF-4B** contains one crystallographically independent Cu^{2+} ion, one hfbba ligand, and one 3-methyl pyridine ligand. Each octahedral Cu^{2+} ion is surrounded by four oxygens from hfbba ligands [Cu−O distance ranges from 2.015(2) to 2.039(2) Å] and one nitrogen from 3-methyl pyridine ligand [Cu−N distance = 1.966(2) Å] as shown in Figure 2. Both Cu^{2+} centers of **Cu-*F*-MOF-4B** have almost the same coordination environments with a nearly ideal square-pyramidal sphere ($\tau \approx 0$)[19]

dx.doi.org/10.1021/cg101414x |*Cryst. Growth Des.* 2011, 11, 1215–1222

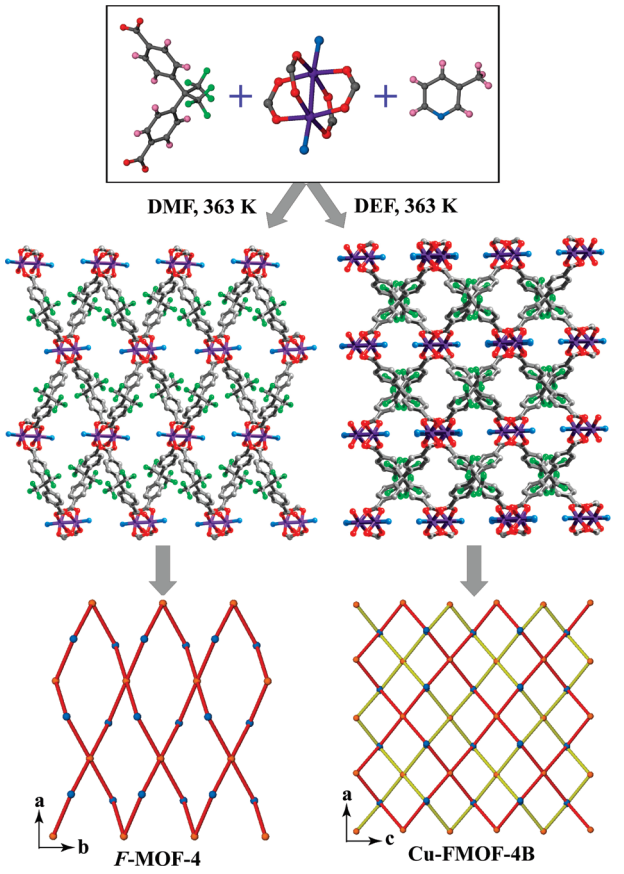

Figure 3. Formation of two isomeric frameworks. ***F*-MOF-4** shows formation non-interdigitated square shaped pores and **Cu-*F*-MOF-4B** shows the formation of square-shaped pores with interdigitated layered structure. Color code: M (violet), N (blue), O (red), C (gray), F (light green).

enclosed by four hfbba ligands [Cu−O distance ranges from 2.015(2) to 2.039(2) Å] and one 3-methyl pyridine ligand [Cu−N distance = 1.966(2) Å]. The dicopper paddlewheel SBU[20] for **Cu-*F*-MOF-4B** with a Cu···Cu distance of 2.678(1) Å is shown in Figure 2b, expanded to show the four hfbba ligands, each coordinated to a dicopper paddlewheel unit via one of their carboxylate groups. Coligand 3-mepy molecules are assembled at the top and bottom position. This dicopper paddlewheel extends further in the *ac* plane to connect the next SBU giving rise to square-shaped pores through the *b* axis and further the 2D structure. 3-mepy molecules are interdigitated into the square-shaped pores along the ac plane. A space filling model shows the assembly of the square-shaped pores to form a one-dimensional (1D) channel (Figure 1). Topological simplification of **Cu-*F*-MOF-4B**, by joining only Cu^{2+} centers, with ligand atoms, shows the formation of square-shaped pores and mode of attachment of ligands with a metal center (Figure 3). This figure shows the interdigitation of two separate layers along the crystallographic *b* axis blocking the pores. In the 2D structure of **Cu-*F*-MOF-4B**, separate layers are arranged in an offset fashion (Figure 3). Each layer is displaced from its adjacent layer by a distance of 2.0182 Å. The -CF_3 groups of H_2hfbba ligands are directed to the outside of the square channels, while DEF molecules occupy the interlayer region. The pore diameter for **Cu-*F*-MOF-4B** is ∼3.106 Å across, based on the largest sphere that could fit into the pore and also remain in contact with van der Waals surface.[21]

Crystal Structures of [Cu_2(hfbba)$_2$(3-mepy)$_2$]. (DMF)$_2$(3-mepy) (F-MOF-4). In the crystal structure of ***F*-MOF-4** (space group $P2_1/c$),[9b] both Cu^{2+} centers have almost the same coordination environment like **Cu-*F*-MOF-4B** with a nearly ideal square pyramidal sphere enclosed by two hfbba ligands and one 3-methyl-pyridine ligand. The dicopper paddlewheel SBU for ***F*-MOF-4** with a Cu···Cu distance of 2.654 Å and two 3-methyl-pyridine ligands occupying the axial positions is shown in Figure 2b. Each H_2hfbba ligand coordinates to another paddlewheel unit, generating the extended corrugated 2D sheets as shown in Figure 3. In ***F*-MOF-4**, the sheets stack along the *y*-axis affording square-shaped cavities along the *c* axis that run through the gross structure (Figure 3). The -CF_3 groups of H_2hfbba ligands are directed to the outside of the larger square channels, whereas DMF and 3-picoline guests reside inside the square-shaped and hexagonal channels. The pore diameter is approximately ∼3.214 Å across, based on the largest sphere that could fit into the pore and be in contact with the van der Waals surface.

Structural comparison between ***F*-MOF-4** and **Cu-*F*-MOF-4B** indicates that a change in solvent of synthesis (DMF and DEF) resulted into diverse changes in resultant MOF architecture. Tetradentate bridging mode of H_2hfbba ligand coordinates with metal centers resulting in the formation of bimetallic tetracarboxylate clusters in all the *F*-MOFs, where apical positions are occupied by 3-picoline resulting into the formation of 2-fold parallel 2D → 2D interpenetration or interdigitation with a 1D channel through crystallographic planes. It is well-known that bimetallic clusters formed by the coordination of ligands and coligands play an important role in the determination of the structure of the resultant framework. In the structure of these three *F*-MOFs, only $\mu_2{}^b$-OCO (Figure 2a) coordination mode is observed, although 10 possible coordination modes exist (see Scheme 1 in Supporting Information, for all possible coordination modes formed by H_2hfbba). As discussed earlier, these *F*-MOFs have same SBUs and coordination sphere; still resultant structures are totally different from each other. ***F*-MOF-4**, synthesized from DMF, has a non-interdigitated 2D structure and **Cu-*F*-MOF-4B**, synthesized from DEF, has a interdigitated structure (Figure 3). We could synthesize a Zn analogue of **Cu-*F*-MOF-4B** by changing the metal source to $Zn(NO_3)_2$ from $Cu(NO_3)_2$ and using similar synthetic conditions. **Cu-*F*-MOF-4B** and **Zn-*F*-MOF-4B**, containing Cu^{2+} and Zn^{2+} metal centers, have significant structural similarity [$a \sim 21.626(2)$ Å, $b \sim 14.662(17)$ Å, $c \sim 17.777(3)$ Å, $\alpha = \beta = \gamma = 90°$, $V \sim 5636.8$ Å^3].

Thermal Stability and PXRD Analysis. We prepared the *F*-MOFs at the gram scale to allow detailed investigation of the aforementioned properties and to examine the architectural and thermal stability of reported in this paper. Thermal gravimetric analysis (TGA) performed on as-synthesized **Cu-*F*-MOF-4B**, **Zn-*F*-MOF-4B**, and ***F*-MOF-4** revealed that these compounds have high thermal stability (see section S3 in Supporting Information, for all data and interpretations regarding guest mobility and thermal stability of these MOFs). The TGA trace for ***F*-MOF-4** showed a gradual weight loss step of ∼20.5% (20−250 °C), corresponding to escape of all *N*,*N*-dimethylformamide (DMF) in the pores (3 DMF; calcd. ∼14%) followed by a sharp weight loss (250−450 °C) probably due to the decomposition of the coordinated 3-picoline molecules before decomposition of

the framework. The TGA analysis of **Cu-*F*-MOF-4B** show the sharp weight loss of ~17.5% (20−250 °C) corresponding to escape of all guest solvent molecules in pores followed by a plateau before a sharp weight loss (250−390 °C) probably due to the decomposition of the coordinated 3-methyl pyridine molecules. After 300 °C framework decomposes completely giving 40% residue. Also TGA traces of **Zn-*F*-MOF-4B** shows a sharp weight loss of 16.5% (185−245 °C) corresponding to the escape of all guest solvent molecules from rigid framework followed by a plateau before a sharp weight loss (235−265 °C) giving 30% residue after decomposition of the framework.

In order to confirm the phase purity of the bulk materials, PXRD experiments were carried out on all complexes. The PXRD of DCM exchanged, as synthesized experimental and computer-simulated patterns of all of *F*-MOFs are shown in Supporting Information (Figure S1−S6). As shown in figures, all major peaks of experimental powder X-ray patterns (PXRDs) of compounds **Cu-*F*-MOF-4B**, **Zn-*F*-MOF-4B**, and ***F*-MOF-4** matches quite well with that of simulated PXRDs, indicating their reasonable crystalline phase purity. The experimental pattern of ***F*-MOF-4** has a few diffraction lines that are unindexed and some that are slightly broadened in comparison with those simulated patterns. This is probably due to the loss of DMF molecules from the lattice or phase change due to grinding during analysis.

H_2 and CO_2 Adsorption. We concentrated on the gas adsorption studies of these *F*-MOFs as from single-crystal diffraction analysis it was revealed that all the *F*-MOFs have the small pores of 3−4 Å. Recently, researchers found that solvent-free frameworks are more useful for gas adsorption. To acquire solvent-free framework, as-synthesized samples of **Cu-*F*-MOF-4B**, **Zn-*F*-MOF-4B**, and ***F*-MOF-4** were immersed in dry dichloromethane at ambient temperature for 72 h, evacuated at ambient temperature for 24 h, then at an elevated temperature 100 °C for 36 h under ultrahigh vacuum (10^{-8} mbar) overnight. Samples thus obtained were optimally evacuated, as evidenced by their well-maintained PXRD patterns and the long plateau (ambient temperature to 325 °C) in their TGA traces (see Figure S2, S4, and S6 in Supporting Information).

As the kinetic diameter of N_2 (3.6 Å) is higher than the pore size of all these *F*-MOFs, these *F*-MOFs are nonporous to N_2. Further, the low kinetic energy of the N_2 molecules at 77 K results in N_2 molecules being unable to effectively enter small pores. However, these *F*-MOFs are able to take the H_2 (2.89 Å) and CO_2 (3.4 Å) as they have a lower kinetic diameter than pore size. All these *F*-MOFs show reversible type I H_2 and CO_2 adsorption isotherms at 77 K and 298 K, respectively. ***F*-MOF-4** shows the highest reversible type I H_2 and CO_2 adsorption in this series, that is, 0.58 wt % and 1.27 mmol/g as pressure approaches to 1 atm as shown in Figure 4. Isostructural **Cu-*F*-MOF-4B** and **Zn-*F*-MOF-4B** show nearly same 0.52 and 0.45 wt % of H_2 uptake, and 0.96 and 0.87 mmol/g of CO_2 adsorption. These results are well anticipated as ***F*-MOF-4** contains the robust paddlewheel Cu^{2+} motif with non-interdigitated layers, which are well separated giving considerable interlayer void space. As a result, the pores are more accessible toward gases. On the other hand **Cu-*F*-MOF-4B**, **Zn-*F*-MOF-4B** has 2D structures with interdigitation of layers resulting in a decrease in interlayer void space.

Magnetic Properties of F-MOF-4 and Cu-FMOF-4B. Both ***F*-MOF-4** and **Cu-*F*-MOF-4B** contain the same dicopper paddlewheel SBU as joints and hfbba ligand as links between joints. However, the distance of these dicopper paddlewheel SBUs with

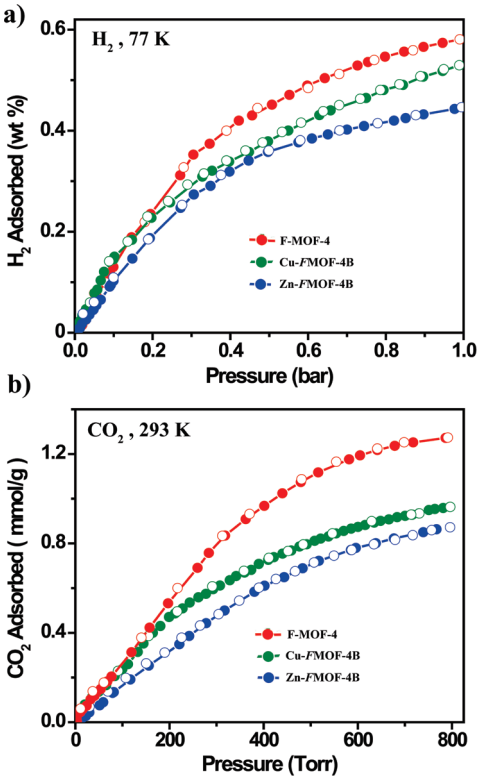

Figure 4. (a) H_2 (77 K) and (b) CO_2 (293 K) isotherm of the *F*-MOFs reported in the paper. Filled and open symbols represent adsorption and desorption branches, respectively.

respect to each other is different due to structural variation. As a result, we anticipated a difference in magnetic behavior of these two *F*-MOFs. Temperature dependence of ZFC and FC molar magnetic susceptibility (χ) for ***F*-MOF-4** shows the overlapping of ZFC and FC on each other in the measured temperature range (Figure 5b). The effective magnetic moment μ_{eff} vs T curve shows a sharply decreasing trend in μ_{eff} with decreasing temperature probably due to an antiferromagnetic (AFM) superexchange (SE) interaction between Cu^{2+} ions. At 300 K, value of μ_{eff} is 1.16 μ_B/Cu atom which is less than the theoretical calculated value for one Cu^{2+} ion (1.73 μ_B), indicating the presence of AFM interactions. The lower value of μ_{eff} indicates onset of AFM ordering. This curve shows two anomalies (change of slope) around 195 and 80 K. The value of χT at 300 K is 0.67 emu mol^{-1} K and decreases with decreasing temperature until the lowest measured temperature. A well-defined hysteresis loop is also observed at 10 K, with a coercivity value of 55 Oe (inset of Figure 5b). The opening of the hysteresis indicates the presence of weak ferromagnetic (FM) behavior. As discussed earlier, the origin of FM behavior might be due to canted arrangement of spins introduced by spin frustration.

Temperature dependence of ZFC and FC molar magnetic susceptibility (χ) for **Cu-*F*-MOF-4B** also shows the overlapping of ZFC and FC on each other in the measured temperature range (Figure 5d). The effective magnetic moment μ_{eff} vs T curve shows a sharply decreasing trend in μ_{eff} with decreasing temperature probably due to an AFM SE interaction between Cu^{2+} ions. At 300 K, the value of μ_{eff} per Cu atom in case of **Cu-*F*-MOF-4B** (0.7 μ_B) is less than the ***F*-MOF-4** (1.16 μ_B). It is known that any magnetic interaction get weaken with increasing distance between paramagnetic metal centers (Cu). As the

dx.doi.org/10.1021/cg101414x |*Cryst. Growth Des.* 2011, 11, 1215–1222

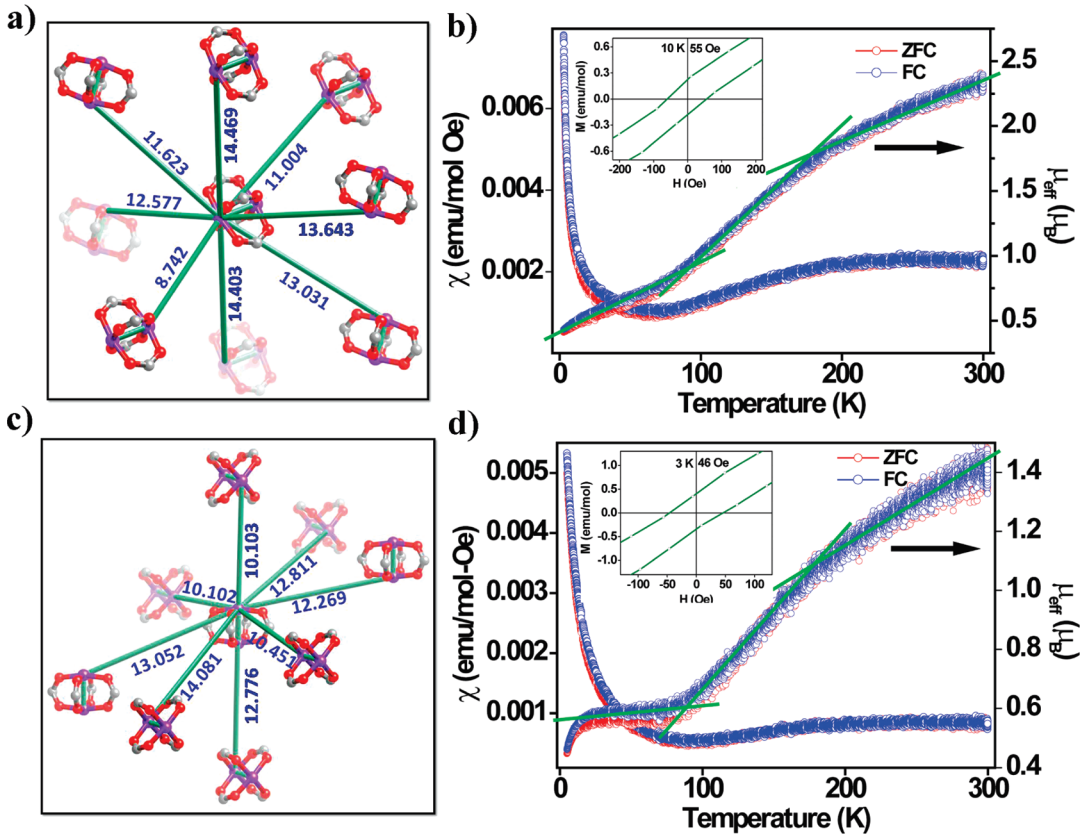

Figure 5. Magnetic properties of *F*-MOFs. (a) Distances between dicopper paddlewheel SBUs in ***F*-MOF-4** ranging from 8.742 to 14.469 Å. (b) The temperature dependence of the magnetic susceptibility χ (left axis), the effective magnetic moment μ_{eff} (right axis) for ***F*-MOF-4**, inset shows the opening of hysteresis loop at 10 K and 55 Oe. (c) Distances between dicopper paddlewheel SBUs in **Cu-*F*-MOF-4B** ranging from 10.102 to 14.081 Å. (d) The temperature dependence of the magnetic susceptibility χ (left axis), the effective magnetic moment μ_{eff} (right axis) for **Cu-*F*-MOF-4B**, inset shows the opening of hysteresis loop at 3 K and 46 Oe. (Light green colored solid lines represent distances between copper−copper metal centers. Color code: violet-copper, gray-carbon, red-oxygen).

distance between the neighboring dicopper paddlewheel SBU is much larger in the case of **Cu-*F*-MOF-4B** (10.102−14.081 Å) (Figure 5c), so the magnetic interaction between them is weaker compared to ***F*-MOF-4** (8.742−14.469 Å) (Figure 5a), which leads to decrease in value of μ_{eff} per Cu atom in **Cu-*F*-MOF-4B**. Like the case of ***F*-MOF-4**, the curve shows anomalies (change of slope) around 195 and 80 K; additionally it shows another anomaly around 20 K, and a sudden decrease in the value of μ_{eff} is observed. A well-defined hysteresis loop is also observed at 3 K (a temperature value lower than for ***F*-MOF-4** due to reduced magnetic interactions), with a coercivity value of 46 Oe (inset of Figure 5d). The opening of the hysteresis indicates the presence of FM behavior. This magnetic response may reflect a situation in which the spins increasing tend to align in an antiparallel fashion but with decreasing thermal activation energy; this ordering apparently comes to a halt due to geometric spin frustration. As a result of this, the effective magnetic moment μ_{eff} ceases to decrease in this temperature region upon further cooling. It can be noted here that μ_{eff} adopts an almost constant value of approximately 0.58 μ_B between 75 and 20 K. This "paramagnetic ledge"[22] is less pronounced or absent in the case of ***F*-MOF-4**.

CONCLUSION

In conclusion, we have presented three *F*-MOFs with layered structure by using a predesigned perfluorinated bent ligand with N donor ligand and transition metal centers. The coordination mode for all of these *F*-MOFs is μ_2-OCO, although $hfbba^{-2}$ ligand can coordinate in 10 different modes. We noticed that a change in solvent for the synthesis of polymeric frameworks results in diverse changes in the resultant materials possibly due to the different degree of deprotonation of H_2hfbba under appropriate conditions. All these *F*-MOFs show good thermal stability at elevated temperature and comparable H_2 and CO_2 adsorption with reported MOFs. Cu^{2+} shows dominantly antiferromagnetic coupling followed by the appearance of weak ferromagnetic interaction at low temperature in both ***F*-MOF-4** and **Cu-*F*-MOF-4B**. We are continuing our efforts for the synthesis of new polymeric frameworks using N donor monodentate ligands such as 3-pyridine carbonitrile, 3-bromo pyridine, etc., which induces $\pi-\pi$ stacking interactions.

ASSOCIATED CONTENT

Supporting Information. Description of experimental details, including synthetic methods, crystallography, supplementary figures, including TGA, infrared spectroscopy, powder XRD profiles, tables of crystallographic data, CIF files, and anisotropic thermal ellipsoids for *F*-MOFs reported in this paper. This material is available free of charge via the Internet at http://pubs.acs.org.

AUTHOR INFORMATION

Corresponding Author

*E-mail: r.banerjee@ncl.res.in. Fax: + 91-20-25902636. Tel: + 91-20-25902535.

ACKNOWLEDGMENT

P.P. acknowledges CSIR for a project assistantship (PA-II) from CSIR's XIth Five Year Plan Project (NWP0022-H). R.B. acknowledges Dr. S. Pal, Director, NCL for in house project (MLP020626) and CSIR's XIth Five Year Plan Project (Grant No. NWP0022-H) for funding and also Dr. B. D. Kulkarni, Dr. S. Sivaram, and Dr. K. Vijaymohanan for their encouragement. R.B. acknowledges Dr. Saeed Khan (UCLA) for his help in crystallography. Financial assistance from the DST (SR/S1/IC-22/2009) and (SR/S5/NM-104/2006) is acknowledged.

REFERENCES

(1) (a) Kitagawa, S.; Kitaura, R.; Noro, S.-i. *Angew. Chem.* **2004**, *116*, 2388. (b) Ferey, G. *Stud. Surf. Sci. Catal.* **2007**, *170A*, 66.(c) Mueller, U.; Schubert, M. M.; Yaghi, O. M. In *Handbook of Heterogeneous Catalysis*, 2nd ed.; Ertl, G., Knozinger, H., Schuth, F., Weitkamp, J., Eds.; Wiley-VCH: Weinheim, 2008; Vol. 1, p 247. (d) Kaskel, S. In *Handbook of Porous Solids*; Schuth, F.; Sing, K. S. W.; Weitkamp, J., Eds.; Wiley-VCH: Weinheim, 2002; Vol. 2, p 1190. (e) Ranjani, V.; Siriwardane, M.-S. S.; Fisher, E. P.; Poston, J. A. *Energy Fuels* **2001**, *15*, 279. (f) Himeno, S.; Komatsu, T.; Fujita, S. *J. Chem. Eng. Data* **2005**, *50*, 369.

(2) (a) Eddaoudi, M.; Kim, J.; Rosi, N.; Vodak, D.; Wachter, J.; O'Keeffe, M.; Yaghi, O. M. *Science* **2002**, *295*, 469. (b) Kitagawa, S.; Kitaura, R.; Noro, S.-I. *Angew. Chem., Int. Ed.* **2004**, *43*, 2334. (c) Matsuda, R.; Kitaura, R.; Kitagawa, S.; Kubota, Y.; Belosludov, R. V.; Kobayashi, T. C.; Sakamoto, H.; Chiba, T.; Takata, M.; Kawazoe, Y.; Mita, Y. *Nature* **2005**, *436*, 238. (d) Millward, A. R.; Yaghi, O. M. *J. Am. Chem. Soc.* **2005**, *127*, 17998. (e) Furukawa, H.; Miller, M. A.; Yaghi, O. M. *J. Mater. Chem.* **2007**, *17*, 3197. (f) Ferey, G. *Chem. Soc. Rev.* **2008**, *37*, 191. (g) Ma, S.; Sun, D.; Simmons, J. M.; Collier, C. D.; Yuan, D.; Zhou, H.-C. *J. Am. Chem. Soc.* **2008**, *130*, 1012. (h) Morris, R. E.; Wheatley, P. S. *Angew. Chem., Int. Ed.* **2008**, *47*, 4966. (i) Llewellyn, P. L.; Bourrelly, S.; Serre, C.; Vimont, A.; Daturi, M.; Hamon, L.; De Weireld, G.; Chang, J.-S.; Hong, D.-Y.; Hwang, Y. K.; Jhung, S. H.; Ferey, G. *Langmuir* **2008**, *24*, 7245. (j) Murray, L. J.; Dinca, M.; Long, J. R. *Chem. Soc. Rev.* **2009**, *38*, 1294. (k) Chen, B.; Xiang, S.; Qian, G. *Acc. Chem. Res.* **2010**, *43*, 1115.

(3) (a) Li, D.; Kaneko, K. *Chem. Phys. Lett.* **2001**, *335*, 50. (b) Bourrelly, S.; Llewellyn, P. L.; Serre, C.; Millange, F.; Loiseau, T.; Ferey, G. *J. Am. Chem. Soc.* **2005**, *127*, 13519. (c) Millward, A. R.; Yaghi, O. M. *J. Am. Chem. Soc.* **2005**, *127*, 17998. (d) Ferey, G.; Serre, C.; Mellot-Draznieks, C.; Millange, F.; Surble, S.; Dutour, J.; Margiolaki, I. *Angew. Chem., Int. Ed.* **2004**, *43*, 6296. (e) Ferey, G.; Mellot-Draznieks, C.; Serre, C.; Millange, F.; Dutour, J.; Surble, S.; Margiolaki, I. *Science* **2005**, *309*, 2040.(f) Snurr, R. Q.; Hupp, J. T.; Nguyen, S. T. *50* 2004, *6*. (g) Llewellyn, P. L.; Bourrrelly, S.; Serre, C.; Filinchuk, Y.; Ferey, G. *Angew. Chem., Int. Ed.* **2006**, *45*, 7751. (h) Rowsell, J. L. C.; Yaghi, O. M. *Microporous Mesoporous Mater.* **2004**, *73*, 3. (i) Kitagawa, S.; Kitaura, R.; Noro, S. *Angew. Chem., Int. Ed.* **2004**, *43*, 2334. (j) Snurr, R. Q.; Hupp, J. T.; Nguyen, S. T. *AlChE J.* **2004**, *50*, 1090.

(4) (a) Forster, P. M.; Cheetham, A. K. *Top. Catal.* **2003**, *24*, 79. (b) Farrusseng, D.; Aguado, S.; Pinel, C. *Angew. Chem., Int. Ed.* **2009**, *48*, 7502. (c) Wang, Z.; Chen, G.; Ding, K. *Chem. Rev.* **2009**, *109*, 322. (d) Farrusseng, D.; Aguado, S.; Pinel, C. *Angew. Chem., Int. Ed.* **2009**, *48*, 7502. (e) Lee, J.; Farha, O. K.; Roberts, J.; Scheidt, K. A.; Nguyen, S. T.; Hupp, J. T. *Chem. Soc. Rev.* **2009**, *38*, 1450. (f) Ingleson, M. J.; Barrio, J. P.; Bacsa, J.; Dickinson, C.; Park, H.; Rosseinsky, M. J. *Chem. Commun.* **2008**, 1287.

(5) (a) Janiak, C. *Dalton Trans.* **2003**, 2781. (b) Maspoch, D.; Ruiz-Molina, D.; Veciana, J. *Chem. Soc. Rev.* **2007**, *36*, 770. (c) Ramesh, R. *Nature* **2009**, *461*, 1218. (d) Jain, P.; Ramachandran, V.; Clark, R. J.; Zhou, H. D.; Toby, B. H.; Dalal, N. S.; Kroto, H. W.; Cheetham, A. K. *J. Am. Chem. Soc.* **2009**, *131*, 1362. (e) Zhang, W.; Ye, H.-Y.; Cai, H.-L.; Ge, J.-Z.; Xiong, R.-G.; Huang, S. D. *J. Am. Chem. Soc.* **2010**, *132*, 7300. (f) Zhang, X. X.; Chui, S. S.-Y.; Williams, I. D. *J. Appl. Phys.* **2000**, *87*, 6007. (g) Moulton, B.; Lu, J.; Hajndl, R.; Hariharan, H.; Zaworotko, M. J. *Angew. Chem., Int. Ed.* **2002**, *41*, 2821.

(6) (a) Horcajada, P.; Chalati, T.; Serre, C.; Gillet, B.; Sebrie, C.; Baati, T.; Eubank, J. F.; Heurtaux, D.; Clayette, P.; Kreuz, C.; Chang, J. S.; Hwang, Y. K.; Marsaud, V.; Bories, P. N.; Cynober, L.; Gil, S.; Ferey, G.; Couvreur, P.; Gref, R. *Nat. Mater.* **2010**, *9*, 172. (b) Horcajada, P.; Serre, C.; Vallet-Regi, M.; Sebban, M.; Taulelle, F.; Ferey, G. *Angew. Chem., Int. Ed.* **2006**, *45*, 5974. (c) Dupuis, A.; Guo, N.; Gao, Y.; Godbout, N.; Lacroix, S.; Dubois, C.; Skorobogatiy, M. *Opt. Lett.* **2007**, *32*, 109. (d) Hinks, N. J.; McKinlay, A. C.; Xiao, B.; Wheatley, P. S.; Morris, R. E. *Microporous Mesoporous Mater.* **2010**, *129*, 330. (e) Horcajada, P.; Serre, C.; Maurin, G.; Ramsahye, N. A.; Balas, F.; Vallet-Regí, M. A.; Sebban, M.; Taulelle, F.; Férey, G. R. *J. Am. Chem. Soc.* **2008**, *130*, 6774.

(7) (a) An, J.; Geib, S. J.; Rosi, N. L. *J. Am. Chem. Soc.* **2009**, *132*, 38. (b) An, J.; Rosi, N. L. *J. Am. Chem. Soc.* **2010**, *132*, 5578. (c) Pan, L.; Sander, M. B.; Huang, X.; Li, J.; Smith, M.; Bittner, E.; Bockrath, B.; Johnson, J. K. *J. Am. Chem. Soc.* **2004**, *126*, 1308. (d) Hulvey, Z.; Falcao, E. H. L.; Eckert, J.; Cheetham, A. K. *J. Mater. Chem.* **2009**, *19*, 4307. (e) Park, K. S.; Ni, Z.; Cote, A. P.; Choi, J. Y.; Huang, R.; Uribe-Romo, F. J.; Chae, H. K.; O'Keeffe, M.; Yaghi, O. M. *Proc. Natl. Acad. Sci.* **2006**, *103*, 10186. (f) Banerjee, R.; Phan, A.; Wang, B.; Knobler, C.; Furukawa, H.; O'Keeffe, M.; Yaghi, O. M. *Science* **2008**, *319*, 939. (g) Ma, S.; Zhou, H.−C. *J. Am. Chem. Soc.* **2006**, *128*, 11734. (h) An, J.; Rosi, N. L. *J. Am. Chem. Soc.* **2010**, *132*, 5578. (i) Chen, B.; Ockwig, N. W.; Millward, A. R.; Contreras, D. S.; Yaghi, O. M. *Angew. Chem., Int. Ed.* **2005**, *44*, 4745. (j) Lin, J.-B.; Zhang, J.-P.; Chen, X.-M. *J. Am. Chem. Soc.* **2010**, *132*, 6654. (k) Sun, D.; Ma, S.; Ke, Y.; Collins, D. J.; Zhou, H.-C. *J. Am. Chem. Soc.* **2006**, *128*, 3896. (l) Yang, Q.; Zhong, C. *J. Phys. Chem. B* **2005**, *110*, 655.

(8) (a) Chun, H.; Dybtsev, D. N.; Kim, H.; Kim., K. *Chem.—Eur. J.* **2005**, *11*, 3521. (b) Hulvey, Z.; Falcao, E. H. L.; Eckert, J.; Cheetham, A. K. *J. Mater. Chem.* **2009**, *19*, 4307. (c) Lee, J. Y.; Li, J.; Jagiello, J. *J. Solid State Chem.* **2005**, *178*, 2527. (d) Yang, W.; Lin, X.; Blake, A. J.; Wilson, C.; Hubberstey, P.; Champness, N. R.; Schroder, M. *Inorg. Chem.* **2009**, *48*, 11067. (e) Fernandez, C. A.; Thallapally, P. K.; Motkuri, R. K.; Nune, S. K.; Sumrak, J. C.; Tian, J.; Liu, J. *Cryst. Growth Des.* **2010**, *10*, 1037. (f) Pan, L.; Sander, M. B.; Huang, X.; Li, J.; Smith, M.; Bittner, E.; Bockrath, B.; Johnson, J. K. *J. Am. Chem. Soc.* **2004**, *126*, 1308. (g) Yang, C.; Wang, X.; Omary, M. A. *J. Am. Chem. Soc.* **2007**, *129*, 15454.

(9) (a) Pachfule, P.; Dey, C.; Panda, T.; Vanka, K.; Banerjee, R. *Cryst. Growth Des.* **2010**, *10*, 1351. (b) Pachfule, P.; Dey, C.; Panda, T.; Vanka, K.; Banerjee, R. *CrystEngComm* **2010**, *12*, 1600.

(10) (a) Ameloot, R.; Gobechiya, E.; Uji-i, H.; Martens, J. A.; Hofkens, J.; Alaerts, L.; Sels, B. F.; De Vos, D. E. *Adv. Mater.* **2010**, *22*, 2685. (b) Horcajada, P.; Serre, C.; Grosso, D.; Boissiere, C.; Perruchas, S.; Sanchez, C.; Ferey, G. *Adv. Mater.* **2009**, *21*, 1931. (c) Tranchemontagne, D. J.; Hunt, J. R.; Yaghi, O. M. *Tetrahedron* **2008**, *64*, 8553. (d) Saha, D.; Deng, S.; Yang, Z. *J Porous Mater.* **2009**, *16*, 141. (e) Farha, O. K.; Hupp, J. T. *Acc. Chem. Res.* **2010**, *43*, 1166. (f) Parnham, E. R.; Morris, R. E. *Acc. Chem. Res.* **2007**, *40*, 1005. (g) Lin, Z.; Wragg, D. S.; Morris, R. E. *Chem. Commun.* **2006**, 2021. (h) Liao, J. H.; Wu, P. C.; Huang, W. C. *Cryst. Growth Des.* **2006**, *6*, 1062. (i) Sheu, C. Y.; Lee, S. F.; Lii, K. H. *Inorg. Chem.* **2006**, *45*, 1891. (j) Tsao, C. P.; Sheu, C. Y.; Nguyen, N.; Lii, K. H. *Inorg. Chem.* **2006**, *45*, 6361. (k) Liao, J. H.; Huang, W. C. *Inorg. Chem. Commun.* **2006**, *9*, 1227. (l) Lin, Z.; Slawin, A. M. Z.; Morris, R. E. *J. Am. Chem. Soc.* **2007**, *129*, 4880. (m) Parnham, E. R.; Morris, R. E. *Acc. Chem. Res.* **2007**, *40*, 1005. (n) Lin, Z.; Wragg, J. E.; Morris, R. E. *J. Am. Chem. Soc.* **2007**, *129*, 10334.

(11) Here it should be noted that fluorinated metal organic framework (*F*-MOF) referred to here is not fully fluorinated but it is the

partially fluorinated where only hydrogen atoms from the isopropyl group are replaced by fluorine.

(12) The abbreviation -4B stands for *F*-MOFs synthesized from DEF. As Cu-*F*MOF-4B has been synthesized from same ingredients as *F*-MOF-4, it has been named Cu-*F*MOF-4B. Also Zn-*F*MOF-4B has been named as it has been synthesized from DEF and with Zn.

(13) *SMART*, Version 5.05; Bruker AXS, Inc.: Madison, WI, 1998.

(14) *SAINT-Plus*, Version 7.03; Bruker AXS Inc.: Madison, Wisconsin, USA, 2004.

(15) Sheldrick, G. M. *SADABS*, Version 2.03 and *TWINABS*, Version 1.02; University of Göttingen: Germany, 2002.

(16) Sheldrick, G. M. *SHELXS '97*; University of Göttingen: Germany, 1997.

(17) Sheldrick, G. M. *SHELXTL '97*; University of Göttingen: Germany, 1997

(18) Spek, A. L. *PLATON, A Multipurpose Crystallographic Tool*; Utrecht University: Utrecht, The Netherlands, 2005.

(19) Addison, A. W.; Rao, T. N.; Reedijk, J.; Rijn, J. V.; Verschoor, G. C. *J. Chem. Soc., Dalton Trans.* **1984**, 1349.

(20) (a) O'Keefe, M.; Eddaoudi, M.; Li, H.; Reineke, T. M.; Yaghi, O. M. *J. Solid State Chem.* **2000**, *152*, 3. (b) Tranchemontagne, D. J.; Mendoza-Cortes, J. L.; O'Keefe, M.; Yaghi, O. M. *Chem. Soc. Rev.* **2009**, *38*, 1257. (c) Mellot-Draznieks, C.; Dutour, J.; Ferey, G. *Angew. Chem., Int. Ed.* **2004**, *43*, 6290. (d) Chen, Z.; Xiang, S.; Arman, H. D.; Li, P.; Tidrow, S.; Zhao, D.; Chen, B. *Eur. J. Inorg. Chem.* **2010**, 3745. (e) Chen, B.; Eddaoudi, M.; Reineke, T. M.; Kampf, J. W.; O'Keeffe, M.; Yaghi, O. M. *J. Am. Chem. Soc.* **2000**, *122*, 11559. (f) Xiang, S.; Zhou, W.; Gallegos, J. M.; Liu, Y.; Chen, B. *J. Am. Chem. Soc.* **2009**, *131*, 12415. (g) Seki, K.; Takamizawa, S.; Mori, W. *Chem. Lett.* **2001**, 332. (h) Seki, K.; Mori, W. *J. Phys. Chem. B* **2002**, *106*, 1380. (i) Kitaura, R.; Iwahori, F.; Matsuda, R.; Kitagawa, S.; Kubota, Y.; Takata, M.; Kobayashi, T. C. *Inorg. Chem.* **2004**, *43*, 6522. (j) Horike, S.; Matsuda, R.; Tanaka, D.; Matsubara, S.; Mizuno, M.; Endo, K.; Kitagawa, S. *Angew. Chem., Int. Ed.* **2006**, *45*, 7226.

(21) All calculations were done using Cerius^2 software (Ver. 4.2, Accelrys); van der Waals radii were taken into consideration in all cases (C, 1.70; H, 1.20; O, 1.52; N, 1.55; Cl, 1.79; Br, 1.89 Å).

(22) Daniel, C.; Hartl, H. *J. Am. Chem. Soc.* **2009**, *131*, 5101.